Bulletin of JSME, Vol. 29, No. 250 April 1986

Paper No. 250—38

Surface Roughening Mechanism of Polycrystalline Metal Sheet during Plastic Deformation*

(Effect of Strain Path on Surface Topography)

By Nozomu KAWAI**, Tamotsu NAKAMURA† and Yūjirō UKAI††

A surface roughening phenomenon was investigated using commercially pure aluminium sheets deformed plastically along various proportional strain paths. Surface profiles were measured in three directions of a major principal strain ε_1, a minor principal strain ε_2 and 45 degrees to ε_1 direction. The mean value of R_a in the three directions could be expressed by the equation: $\bar{R}_a = 3.14\ \varepsilon_d$, where ε_d is an absolute value of principal strain vector in-plane, independently of the strain path. Both R_a and the wavelength λ_m at spectrum maximum showed a relatively large difference between ε_1 and ε_2 direction in the case of the plane strain path, but no significant difference in every direction in the balanced bi-axial tensile path. The anisotropic geometry of surface topography corresponded with the direction of the maximum shear stress plane in the bulk metal.

Key words: Forming, Polycrystalline Metal Sheet, Surface Roughening, Strain Path, Surface Roughness, Wavelength of Surface Profile

1. Introduction

When a sheet metal with a large grain size is deformed, its free surface shows a rough appearance, called orange peel. The surface roughening phenomenon of the sheet metal may influence the lubricational conditions of the tool-work interface in metal-working processes.

The surface roughening phenomena have been investigated by a number of researchers [1]~[7], who confirmed that the surface roughness was approximately proportional to the strain ε and the average grain diameter d_o, when a polycrystalline metal sheet is deformed. However, the three-dimensional geometry of the topography of the roughened surface has not been sufficiently examined yet.

The surface roughening mechanism of a polycrystalline metal sheet was investigated in detail in the present paper, using commercially pure aluminium sheets deformed plastically along various strain paths. The surface profiles were measured in three directions, and the center line average roughness R_a and the main wavelength λ_m of these profiles were determined. The effect of a slip deformation in the subsurface grains on the surface roughening was also investigated.

* Received 16th October, 1984.
** Professor, Faculty of Engineering, Nagoya University, Furō-chō, Chikusa-ku, Nagoya, Japan.
† Assistant Professor, Faculty of Engineering, Shizuoka University, 3-5-1 Jōhoku, Hamamatsu, Japan
†† Aisin Seiki Co., Ltd., Minamikane-chō, Nishio, Japan.

2. Experimental Methods

The tested material was a commercially pure aluminium A 1050 (in JIS) sheet of 0.8 mm in thickness, of which stress-strain relations and plastic strain ratio r are shown in Table 1. The initial surface roughness of the sheet was 0.02 μm in the center line average R_a, and average grain diameter d_o was about 16 μm. Other aluminium sheets with average grain diameter d_o ranging from 0.23 to 0.43 mm (Fig. 1) were also used.

The sheetmetals were deformed along four proportional strain paths: uniaxial tension (principal strain ratio $\beta = -0.5$), plane strain tension ($\beta = 0$), bi-axial tension ($\beta = 0.5$) and balanced bi-axial tension ($\beta = 1$). The uniaxial tensile test was carried out using a tesile test-piece of 13 type in JIS. The other strain paths were attained using the test-piece as shown in Fig. 2 and the bulge test apparatus as shown in Fig. 3. The test-piece is clamped together with a driving plate having a center hole of 12 mm in diameter by means of an annular blank-holder with a bead, and is bulged by a flat bottomed punch. This method was proposed by Marciniak et al.[8] As shown in Fig. 4, the resultant strain paths are approximately linear.

3. Measuring and Analyzing Methods of Surface Topography

To estimate the three-dimensional geometry of the surface topograhy quantitatively, the surface profiles were measured in three directions in-plane on the sheet specimen, that is, the major principal strain ε_1 direction, the minor principal strain ε_2 direction and at 45 degrees in relation to the ε_1 direction. The surface profiles were measured using a stylus-type surface profile

tester, and the surface roughness and wavelength of these surface profile curves were determined. The surface roughness is represented by the center line average R_a (in JIS) with 2 mm of traversing length and 0.25 mm of cut-off length. The surface roughness measured in ε_1, ε_2 and 45 degrees directions are indicated by R_{a1}, R_{a2} and R_{ax}, respectively, and a mean value in-plane $\bar{R}a$ is obtained by the following equation.

$$\bar{R}a = (R_{a1} + R_{a2} + 2R_{ax})/4 \quad \cdots\cdots\cdots(1)$$

To estimate the wavelength of the surface profile curve, a power spectrum of the curve is analyzed using the maximum entropy method (MEM)[9].

Table 1 Plastic properties of testpiece in tensile test

	F MPa	n Value	r Value
0°	174.4	0.285	0.748
45°	155.8	0.276	1.283
90°	165.6	0.284	0.795
Mean	162.7	0.280	1.027

Stress-Strain Relation: $\sigma = F\,\varepsilon^n$
0°, 45° and 90° are angles to R.D.

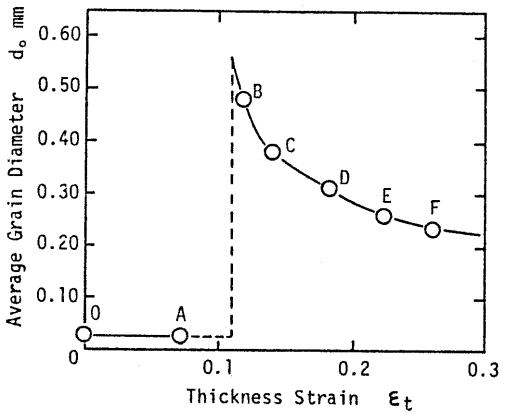

Intermediate Annealing: 400 °C, 1 h
Final Annealing: 450 °C, 1 h

Fig. 1 Relation between thickness strain and average grain diameter

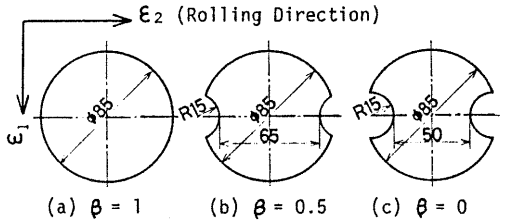

ε_1: Major Strain, ε_2: Minor Strain
$\beta = \varepsilon_2/\varepsilon_1$: Strain Ratio
Initial Thickness: t_o = 0.8 mm

Fig. 2 Testpieces for various strain paths in bulge test

4. Effect of Strain Path on Surface Topography

4.1 Surface Roughness Figure 5 shows the principal strain diagram ε_1 vs. ε_2 where a center line average roughness R_{a1} measured along the major strain ε_1 is plotted. The constant roughness curves shown by the solid lines are not similar to constant equivalent curves. They are rather similar to the diffused necking curve in the region $\beta > 0$ and to a localized necking curve in the region of $\beta < 0$, as pointed out by Kobayashi et al.[1]-[3]

Figure 6 shows the ε_1 vs. ε_2 diagram, where a mean value of the center line average in-plane $\bar{R}a$ is plotted. Again, the constant $\bar{R}a$ curves are not similar to the constant equivalent strain curves, but they resemble the circular curve of the constant absolute value of principal strain vector in-plane, that is, $\varepsilon_d = (\varepsilon_1^2 + \varepsilon_2^2)^{1/2}$. Thus, the mean value of the center line average in-plane $\bar{R}a$ is approximately proportional to the representative strain ε_d, as follows;

$$\bar{R}a = 3.14\,\varepsilon_d. \quad \cdots\cdots\cdots\cdots\cdots(2)$$

Figure 7 shows a relation between the mean value of the center line average roughness in-plane $\bar{R}a$ and the equivalent strain ε_{eq}. It is confirmed that the increasing rate of the mean value of $d\bar{R}a/d\varepsilon_{eq}$ varies siginificantly with the strain path.

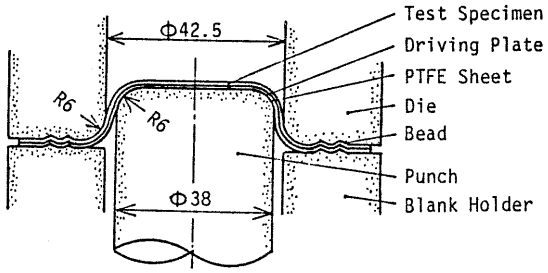

Fig. 3 Bulge test apparatus

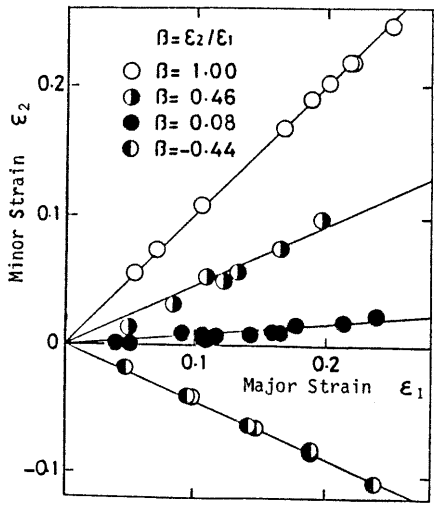

Fig. 4 Strain path measurements

To examine the orientation of the topography of the roughened surface, the difference between R_{a1} and R_{a2}, namely $\Delta R_a = R_{a1} - R_{a2}$, is plotted against the representative strain ε_d in Fig. 8. The value of ΔR_a varies linearly with the strain ε_d except for the case of the balanced bi-axial tension, where ΔR_a equals approximately zero (i.e., the surface topography is isotropic). The increasing rate of ΔR_a, namely $\xi = \Delta R_a/\varepsilon_d$, is defined as an anisotropic parameter of the topography of roughened surface. The value of ξ shows a maximum in the case of plane strain path ($\beta = 0$), and a minimum in the case of uniaxial tensile path ($\beta = -0.5$).

Such an anisotropic topography is illustrated clearly by the pole distribution diagram as shown in Fig. 9 (a) ∿ (c). The surface roughness shows the most prominent anisotropy in the case of the plane strain ($\beta = 0$).

4.2 Wavelength of Surface Profile Curve

Figure 10 (a) and (b) show some examples of the spectrum diagram obtained by analyzing the surface profile curves using the maximum entropy method (MEM). The abscissa represents frequency f 1/mm, which is an inversion of wavelength λ; the ordinate represents a spectrum ratio to the spectrum maximum S_{max}. The main wavelength can be defined clearly as the wavelength λ_m at the spectrum maximum S_{max}, because a sharp maximum peak appears.

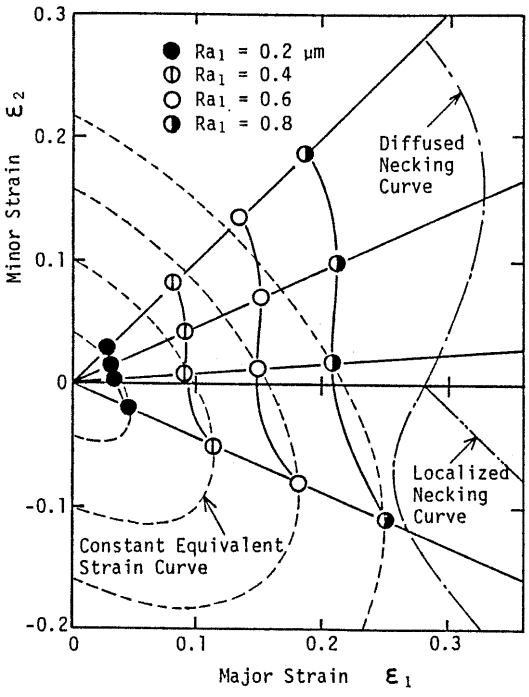

Fig. 5 Constant R_{a1} curve on ε_1 vs. ε_2 diagram

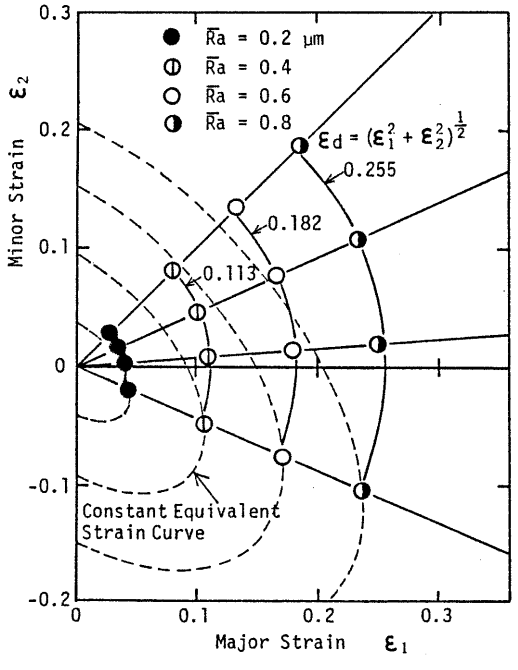

Fig. 6 Constant $\bar{R}_a$ curve on ε_1 vs. ε_2 diagram

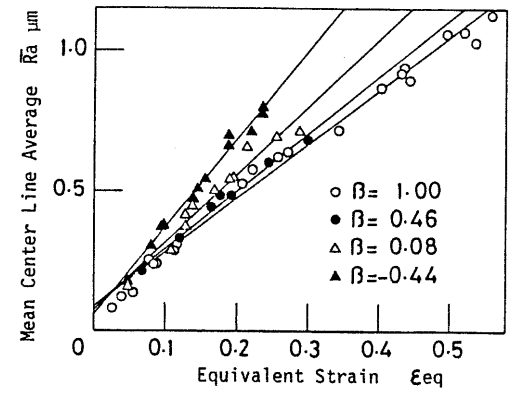

Fig. 7 Relation between $\bar{R}_a$ and ε_{eq}

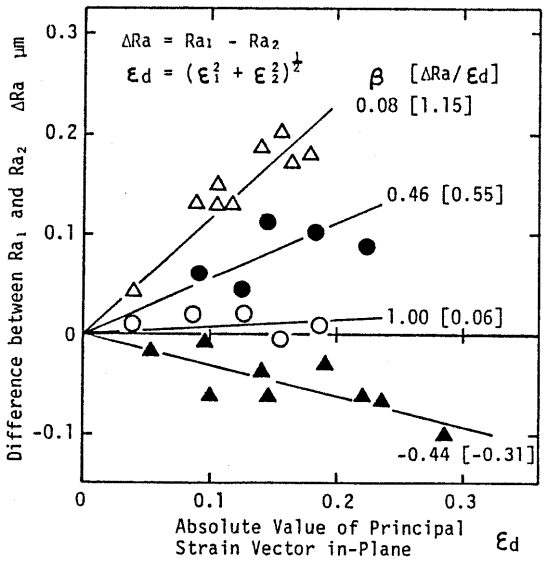

Fig. 8 Variation of difference ΔR_a between R_{a1} and R_{a2} with strain ε_d

Fig. 11 shows a relation between the wavelength λ_m and the representative strain ε_d. The wavelength λ_m in the case of plane strain path is about 200 ∿ 240 μm in the ε_1 direction, and about 400 ∿ 460 μm in the ε_2 direction. These values of wavelength λ_m are about 12 ∿ 15 times and about 26 ∿ 29 times the average grain diameter d_o = 16 μm, respectively. Such an anisotropic property of the wavelength λ_m does not appear in other strain paths. In the case of balanced bi-axial tension, the wavelength λ_m increase gradually with the strain ε_d.

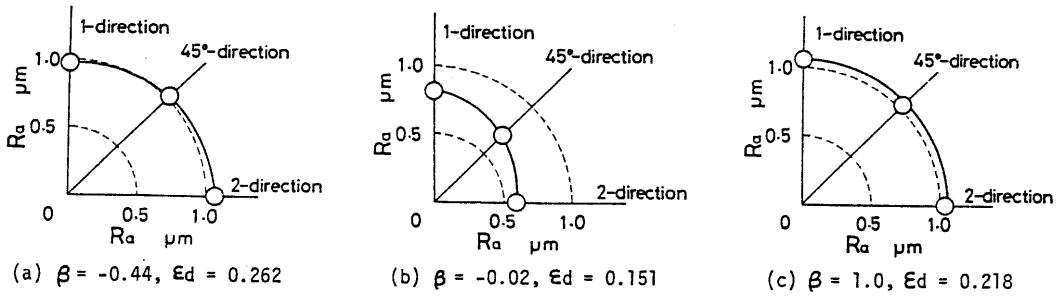

(a) β = -0.44, ε_d = 0.262 (b) β = -0.02, ε_d = 0.151 (c) β = 1.0, ε_d = 0.218

Fig. 9 Pole distribution diagram of center line average R_a

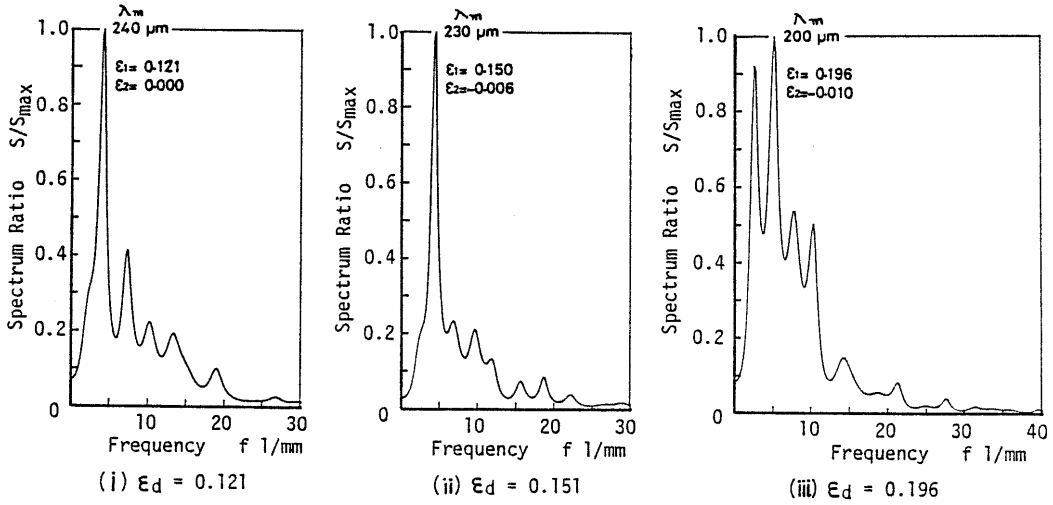

(a) Major Principal Strain ε_1 Direction

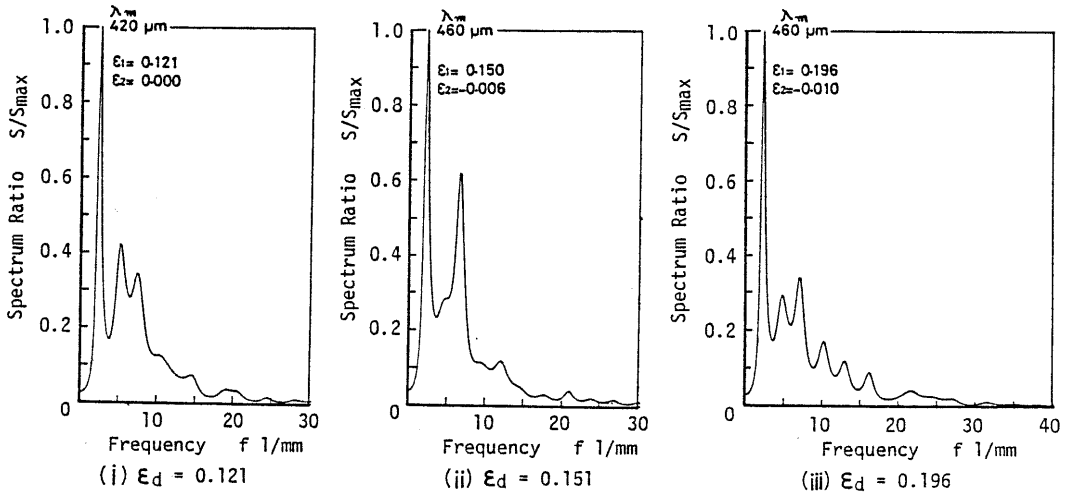

(b) Minor Principal Strain ε_2 Direction

Fig. 10 Spectrum diagram examples by MEM analysis (plane strain path, β = -0.02)

Figure 12 (a) ∿ (c) show the pole distribution diagrams of the wavelength λ_m. It is confirmed from Fig. 9 and 12 that the surface topography roughened in the plane strain path shows a remarkable geometric anisotropy, while the one roughened in the balanced bi-axial tensile path shows a considerable isotropy. It has been clarified in this section that the mean value of the center line average in-plane $\bar{R}_a$ is represented by the same equation regrdless of the surface topography varies remarkably with the strain path.

5. Surface Roughening Mechanism

Using commercially pure aluminium sheets with an average grain diameter d_o of about 16 to 500 μm, the effects of the average number of grains in the thickness direction t_o/d_o on the surface roughening phenomenon are examined. Figure 13 shows a relation between the center line average roughness R_a and the average grain diameter d_o, in the case of $\beta = 1$ and $\varepsilon_d = 0.134$. As pointed out by Osakada et al.[7], R_a is approximately proportional to the average grain diameter d_o, when the diameter d_o is less than 0.3 mm. However, R_a increases rapidly when the diameter d_o exceeds 0.35 mm.

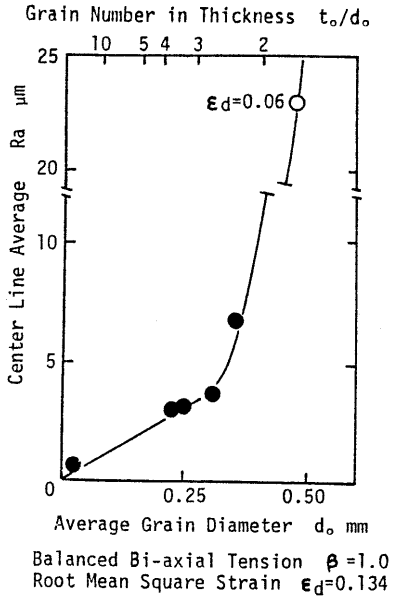

Fig. 13 Relation between center line average R_a and average grain diameter d_o

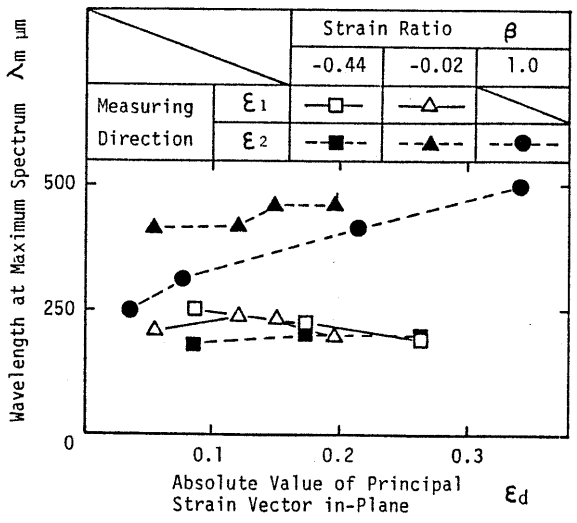

Fig. 11 Relation between wavelength λ_m and strain ε_d

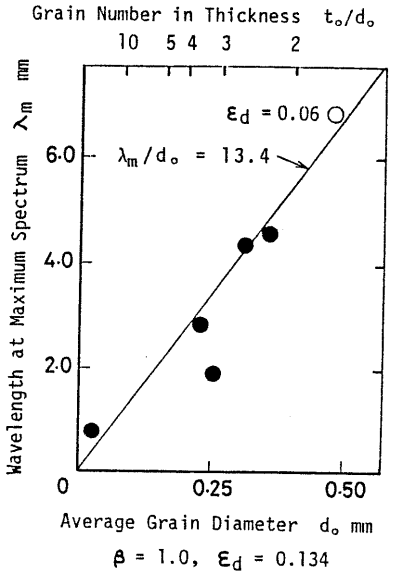

Fig. 14 Relation between wavelength λ_m and average grain diameter d_o

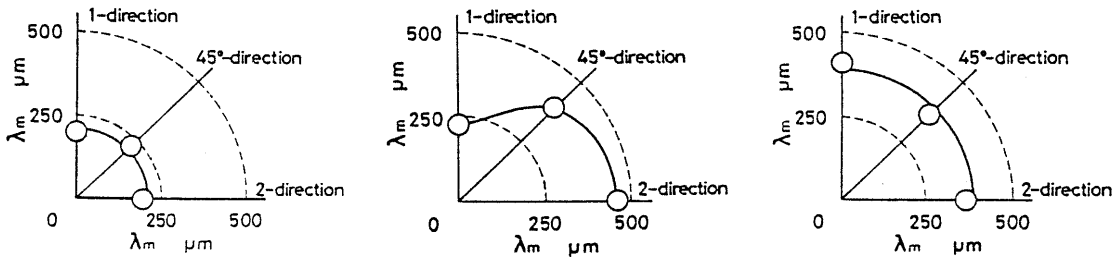

Fig. 12 Pole distribution diagram of wavelength λ_m

This is possibly because localized necking is facilitated by the surface roughening phenomenon as demonstrated by Yamaguchi et al.[5].

Figure 14 shows the relation betweeen the wavelength λ_m at the maximum spectrum and the average grain diameter d_o. The wavelength λ_m increases approximately in proportion to the average grain diameter d_o;

$$\lambda_m/d_o = 13.4 \pm 6.9. \quad \cdots\cdots\cdots\cdots (3)$$

Consequently, the surface roughening phenomenon during plastic deformation is essentially dominated by grain diameter d_o, when the number of grains in the thickness direction t_o/d_o is greater than about three. Thus, it is presumed that the surface roughening is influenced by the plastic deformation in the subsurface layer of two or three grains.

To examine the effect of slip deformation in the surface grains on the surface roughening, slip bands of the surface grains developed by electro-polishing were observed in each strain path. As shown in Fig. 15 (a) ∿ (c), the asperities of the slip bands itself were less than about 1 μm, they were not main components of the surface topography. In the case of the balanced bi-axial tension (a), the slip band appears in various directions at random. On the other hand, the slip bands in the case of plane strain path (b) appear approximately in the ε_2 direction. In the case of uniaxial tension (c), the slip bands appear in two directions at 45 degrees in relation to the ε_1 direction. The directions coincide approximately with the directions of the maximum shear stress plane as shown in Fig. 16.

Therefore, the active slip systems of the subsurface grains may be determined as a first approximation by the macroscopic stress in the polycrystalline metal sheet. The geometric orientation of the topography of the roughened surface is considered to be caused by the restricted directionality of the active slip systems. For example, the isotropic surface topography is formed in the case of $\beta = 1$, because the active slip system originates in random directions, while the anisotropic topography is formed in the case of $\beta = 0$, because the active slip system is restricted to near the ε_2 direction.

6. Conclusions

The surface roughening mechanism was examined using commercially pure aluminium sheets deformed plastically along various proportional strain paths. The surface profiles of the sheets were measured in three directions of a major principal strain ε_1, a minor principal strain ε_2 and at 45 degrees in relation to the ε_1 direction. The center line average roughness R_a and the main wavelength λ_m of these profiles were determined. As a result, the following conclusions were reached.

(1) R_{a1} measured along the major principal strain ε_1 direction was plotted on the ε_1 vs. ε_2 diagram. The constant R_{a1} curve is confirmed to be similar to the diffused necking curve in the region of the principal

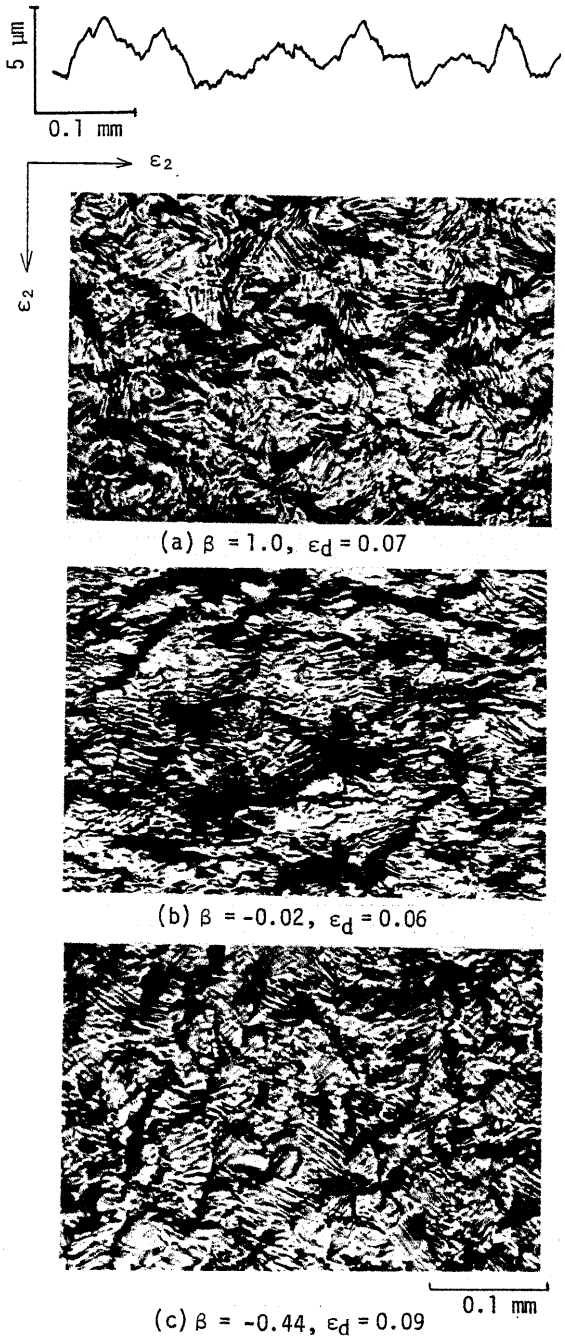

Fig. 15 Surface appearance on slip bands of surface grains in various strain paths

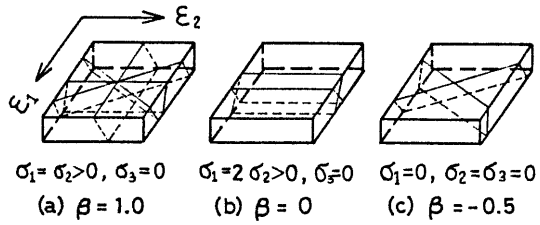

Fig. 16 Maximum shear stress planes in various macroscopic stress state

strain ratio $\beta > 0$, and to the localized necking curve in the region of $\beta < 0$.

(2) The mean value of R_a in-plane is approximately proportional to the absolute value of the strain vector in-plane ε_d regardless of the difference in strain paths.

(3) The difference between R_{a1} in the ε_1 direction and R_{a2} in the ε_2 direction, namely $\Delta R_a = R_{a1} - R_{a2}$, varies linearly with the strain ε_d. The increasing rate of ΔR_a, namely $\xi = \Delta R_a/\varepsilon_d$, could be defined as the anisotropic parameter of the topography of the roughened surface. The value of ξ is maximum in the case of $\beta = 0$, minimum in the case of $\beta = -0.5$, and zero in the case of $\beta = 1$. It has been confirmed that the surface roughness R_a shows a remarkable anisotropy in the case of the plane strain path, while R_a displays a considerable isotropy in the case of the balanced bi-axial tensile path.

(4) The main wavelength λ_m at the spectrum maximum S_{max} is about 12 $\sim$ 16 times the average grain diameter d_o in the case of $\beta = -0.5$. λ_m in the case of $\beta = 0$ is 12 $\sim$ 15 times the value of d_o in the ε_1 direction and 26 $\sim$ 27 times of the value of d_o in the ε_2 direction. It has been confirmed that the wavelength also a remarkable anisotropy in the case of plane strain.

(5) Both R_a and λ_m are approximately proportional to the average grain diameter d_o, when t_o/d_o is greater than about three.

(6) The directions in which the slip bands appear coincide approximately with the directions in which the maximum shear stress planes in the bulk metal intersect with the sheet surface. It is presumed that the anisotropic geometry of the topography of the roughened surface is caused by a restricted directionality of the active slip system.

References

(1) Kobayashi, T. et al., J. of the Japan Society for Technology of Plasticity (in Japanese), Vol. 10, No. 106 (1969), p.793.
(2) Kobayashi, T. et al., ibid, Vol. 11, No. 114 (1970), p. 495.
(3) Kobayashi, T. and Ishigaki, H., ibid, Vol. 15, No. 158 (1974), p. 197.
(4) Fukuda, M. et al., ibid, Vol. 15, No. 167 (1974), p. 994.
(5) Yamaguchi, K. and Mellor, P. B., Int. J. of Mechanical Science, Vol. 18 (1976), p. 85.
(6) Thomson, P. F. and Nayak, P. U., J. of Mechanical Working Technology, Vol. 4, No. 3 (1980), p. 223.
(7) Osakada, K. and Oyane, M., Trans. JSME (in Japanese), Vol. 36, No. 286 (1970), p. 1017.
(8) Marciniak, Z. and Kuczynski, K., Int. J. of Mechanical Science, Vol. 9 (1967), p. 609.
(9) Hino, M., Srectral Analysis, (1978), p. 210, Asakura.